THE JOURNAL OF BIOLOGICAL CHEMISTRY VOL. 286, NO. 35, pp. 30823–30836, September 2, 2011

A Conserved Asparagine Residue in Transmembrane Segment 1 (TM1) of Serotonin Transporter Dictates Chloride-coupled Neurotransmitter Transport*[S]

Received for publication, April 13, 2011, and in revised form, June 30, 2011 Published, JBC Papers in Press, July 7, 2011, DOI 10.1074/jbc.M111.250308

L. Keith Henry,[a,b,g1] Hideki Iwamoto,[a] Julie R. Field,[a] Kristian Kaufmann,[d] Eric S. Dawson,[b,e,f] Miriam T. Jacobs,[c] Chelsea Adams,[g] Bruce Felts,[g] Igor Zdravkovic,[h2] Vanessa Armstrong,[g] Steven Combs,[d] Ernesto Solis,[a3] Gary Rudnick,[c] Sergei Y. Noskov,[h,2,4] Louis J. DeFelice,[a,i3] Jens Meiler,[a,b,d] and Randy D. Blakely[a,i,j5]

From the Departments of [a]Pharmacology, [d]Chemistry, [e]Biochemistry, and [j]Psychiatry, [i]Center for Molecular Neuroscience, [b]Center for Structural Biology, and [f]Vanderbilt Center for Neuroscience Drug Discovery, Vanderbilt University School of Medicine, Nashville, Tennessee 37232-8548, the [c]Department of Pharmacology, Yale University School of Medicine, New Haven, Connecticut 06520-8066, the [g]Department of Pharmacology, Physiology, and Therapeutics, University of North Dakota, Grand Forks, North Dakota 58203, and the [h]Institute for Biocomplexity and Informatics, Department of Biological Sciences, University of Calgary, Calgary, Alberta T2N 1N4, Canada

Na^+- and Cl^--dependent uptake of neurotransmitters via transporters of the SLC6 family, including the human serotonin transporter (SLC6A4), is critical for efficient synaptic transmission. Although residues in the human serotonin transporter involved in direct Cl^- coordination of human serotonin transport have been identified, the role of Cl^- in the transport mechanism remains unclear. Through a combination of mutagenesis, chemical modification, substrate and charge flux measurements, and molecular modeling studies, we reveal an unexpected role for the highly conserved transmembrane segment 1 residue Asn-101 in coupling Cl^- binding to concentrative neurotransmitter uptake.

Chemical signaling by neurotransmitters in the nervous system depends upon the opposing mechanisms of vesicular release and transporter-mediated neurotransmitter clearance (1). In humans, two gene families, designated SLC1 and SLC6, compose the majority of transporters responsible for neurotransmitter inactivation (2–4). Whereas the SLC1 family encodes multiple transporters that inactivate the brain's predominant excitatory neurotransmitter, L-glutamate, the SLC6 gene family includes transporters that clear the brain's major inhibitory neurotransmitters, γ-aminobutyric acid and glycine, as well as transporters for the neurotransmitters dopamine, norepinephrine (NE),[6] and serotonin (5-hydroxytryptamine, 5-HT). The human 5-HT transporter (SLC6A4, hSERT) is of particular clinical significance, being a target for psychostimulants, including cocaine and 3,4-methylenedioxymethamphetamine ("ecstasy"), as well as the site of action for widely prescribed 5-HT selective reuptake inhibitors (5) used in the treatment of mood disorders.

hSERT, like other neurotransmitter transporters of the SLC1 and SLC6 families, displays secondary-active substrate transport (6), coupling the concentrative movement of neurotransmitter to the transmembrane gradients of Na^+ and other ions (7). A distinguishing feature of neurotransmitter transport by the SLC6 family relative to the SLC1 family is a strong dependence on extracellular Cl^- for transport (8, 9). During a single cycle of substrate transport in hSERT, a stoichiometry of 1-5-HT^+_{in}:1-Na^+_{in}:1-Cl^-_{in}:1-K^+_{out} has been advanced on the basis of ion dependence studies in cells and resealed membrane vesicles that predicts an overall electroneutral coupling mechanism. Such studies have led to the belief that the energy stored in the Cl^- concentration gradient contributes directly to transmembrane 5-HT flux (7, 10). However, electrophysiological experiments reveal that SERT can exhibit nonstoichiometric flux states where additional 5-HT-induced charge movements occur (10–13). For the hSERT homolog dopamine transporter, Cl^- has been implicated as a charge carrier in nonstoichiometric flux states, (14, 15) suggesting that the role of Cl^- in neurotransmitter transport is more complex than originally sus-

* This work was supported, in whole or in part, by National Institutes of Health Grants from NIDA (to L. K. H., G. R., and R. D. B.), NINDS (to H. I. and L. J. D.), and NIGMS (to J. M.). This work was also supported by NARSAD (to L. K. H.) and the Center for Structural Biology at Vanderbilt University.

[S] The on-line version of this article (available at http://www.jbc.org) contains supplemental Methods, "Results," Figs. S1–S10, Tables S1–S4, and additional references.

[1] To whom correspondence may be addressed: Dept. of Pharmacology, Physiology, and Therapeutics, University of North Dakota School of Medicine and Health Sciences, Ste. 3700, 501 N. Columbia Rd., Grand Forks, ND 58203. Tel.: 701-777-2295; Fax: 701-777-4490; E-mail: keith.henry@med.und.edu.

[2] Recipient of support from Alberta Heritage Foundation for Medical Research and Discovery Grant from Natural Sciences and Engineering Research Council of Canada.

[3] Present address: Dept. of Physiology and Biophysics, Virginia Commonwealth University, Sanger Hall, 3-038f, Richmond, VA 23298.

[4] Recipient of a scholar award from Alberta Heritage Foundation for Medical Research.

[5] To whom correspondence may be addressed: Center for Molecular Neuroscience, 7140 Medical Research Bldg. III, Vanderbilt University School of Medicine, 465 21st Ave. South, Nashville, TN 37232-8548. Tel.: 615-936-3705; Fax: 615-936-3040; E-mail: randy.blakely@vanderbilt.edu.

[6] The abbreviations used are: NE, norepinephrine; 5-HT, 5-hydroxytryptamine; hSERT, human serotonin transporter; rSERT, rat serotonin transporter; MTS, methanethiosulfonate; MTSET, 2-(trimethylammonium) ethyl methanethiosulfonate bromide; MTSEA, 2-aminoethyl methanethiosulfonate hydrobromide; TM, transmembrane segment; EL, extracellular loop; MD, molecular dynamics simulations; FEP, free energy perturbation; ANOVA, analysis of variance; TEVC, two-electrode voltage clamp; NMDG-Cl, *N*-methyl-D-glucamine-HCl.

pected. Interacting proteins, including syntaxin 1A, can modulate the stoichiometry of charge movements across hSERT and other monoamine transporters (10, 15–17), changes that can alter neuronal firing rates (15, 17). In addition, SERTs are expressed early in the embryo (18, 19), and in many distinct membrane environments (*e.g.* neurons, placenta, lymphoblasts, platelets, and epithelial cells), where Cl^- gradients can change over time (20, 21). Together these findings indicate that the contribution of Cl^- to neurotransmitter transport deserves further investigation.

Recently, high resolution structures of a Cl^--independent SLC6 family member, the leucine transporter from *Aquifex aeolicus* ($LeuT_{Aa}$) (22), has afforded opportunities to elucidate details of neurotransmitter transporter ionic coupling. Although overall sequence identity between $LeuT_{Aa}$ and neurotransmitter transporters is low, amino acid identity approaches 50% for residues surrounding the binding sites for leucine and Na^+, propelling homology-guided structural studies. In addition, crystal structures of the transporters ApcT (23), BetP (24), vSGLT (25), and Mhp1 (26) that have no significant sequence homology to SLC6 family members exhibit the same helical packing pattern as LeuT (27). Therefore, a model-guided study of SLC6 family members may identify important mechanisms that are likely difficult to derive from patterns of sequence conservation.

In a prior study (28), we demonstrated that an asparagine (Asn-101) in hSERT transmembrane segment (TM) 1 tolerates substitution by cysteine and that cells transfected with N101C are sensitive to transport inactivation by positively charged cysteine-directed MTS reagents. Because this inactivation was largely eliminated by the presence of 5-HT, we proposed that Asn-101 might lie at or near the substrate-binding site.

Here, we demonstrate that the Asn-101 residue, homologous to the sodium-coordinating residue Asn-27 in $LeuT_{Aa}$, contributes an important role in facilitating the coupling of Cl^- to 5-HT transport. Rather than directly coordinating Cl^- binding, our evidence indicates that Asn-101 translates Cl^- binding to the stabilization of a TM1–TM6 interhelical network with the participation of TM6 residue Ser-336 to promote efficient coupling between 5-HT and Na^+.

EXPERIMENTAL PROCEDURES

Site-directed Mutagenesis and Construction of Mutant Plasmids—Mutation of hSERT cDNA in pcDNA3.1 or pOTV to generate N101A, N101C, and S336C constructs in hSERT and hSERT C109A backgrounds was performed using the Stratagene QuikChange kit, as described previously (28), with confirmation of all mutants by DNA sequencing (Center for Molecular Neuroscience Neurogenomics, Vanderbilt DNA Sequencing Core Facility or Northwoods DNA, Inc., Bemidji, MN). For cysteine modification studies to probe for Asn-101-sensitive conformational movements, rSERT Asn-101 mutants were generated in the background of Cys substitutions S277C and S404C using a Cys-reduced transporter (X5C; C15A/C21A/C109A/C357I/C622A).

5-HT and NE Transport Measurements—HeLa and HEK-293 cells, maintained at 37 °C in a 5% CO_2-humidified incubator, were grown in complete medium (DMEM, 10% FBS, 2 mM L-glutamine, 100 units/ml penicillin, and 100 μg/ml streptomycin). For initial evaluation of mutant transporter activity, cells were plated at a density of 50,000 cells/cm^2 in 96- or 24-well culture plates. Cells were transfected with hSERT, rSERT, or hNE transporter constructs with TransIT transfection reagent (Mirus Inc., 6 μl per μg of DNA), also in OptiMEM medium as described previously (28), or with Lipofectin followed by infection with vTF7-3 vaccinia virus as described (29). Following transfection (20–48 h), cells were washed with one of the following buffers: MKRHG assay buffer (120 mM NaCl, 4.7 mM KCl, 2.2 mM $CaCl_2$, 1.2 mM $MgSO_4$, 1.2 mM KH_2PO_4, 10 mM glucose, 10 mM HEPES, pH 7.4); chloride-containing assay buffer (5.4 mM potassium gluconate, 1.2 mM calcium gluconate, 7.5 mM HEPES, and either NaCl or NMDG-Cl at 120 mM;) chloride-free assay buffer (same as chloride-containing buffer except 120 mM NaCl is replaced with 120 mM Na*X* (*X* = Br, I, NO_2, NO_3, thiocyanate, acetate, methanesulfonate, or gluconate) and assayed for [^{3}H]5-HT (5-hydroxy[^{3}H]tryptamine-trifluoroacetate, (121 Ci/mmol) Amersham Biosciences) transport as described previously (28). For Na^+ replacements assays, NMDG-Cl was used in place of NaCl. Transport was linear with time under these conditions for up to 15 min. Saturation kinetic profiles for derivation of 5-HT K_m and V_{max} values were established in 24-well plates as described above except 2-fold serial dilutions were used maintaining 5-HT-specific activity, starting at 5 μM of a mixture of labeled and unlabeled 5-HT. Transport assays were terminated by three washes with ice-cold assay buffer, and cells were then dissolved in MicroScint 20 (Packard) scintillation fluid. Uptake from mock-transfected cells was subtracted from transporter-transfected cells to determine specific uptake. Nontransfected cells exhibited comparable uptake to assays performed in the presence of 1 μM paroxetine, 1 μM RTI-55, or 100 nM cocaine. K_m and V_{max} values were derived using a nonlinear curve fit as a function of 5-HT or NE concentration (40 nM to 5 μM) (Prism 4 for Mac, Graphpad software). All experiments were performed in triplicate and repeated in three or more separate assays.

Spontaneous 5-HT Efflux—Cells were loaded as described above for transport studies with 40 nM [^{3}H]5-HT. Loading was allowed to proceed for 30 or 90 min at 37 °C and was terminated by aspiration of assay buffer and a single wash with 0.5 ml of ice-cold MKRHG buffer. MKRHG buffer (0.5 ml) was added to one-half of the wells and returned to 37 °C for 30 min. The wells that did not receive buffer represent the total 5-HT taken up at $T = 0$. Buffer from the efflux wells (representing 5-HT efflux) was collected, transferred to scintillation vials with 5 ml of EcoScint H, and counted. 5-HT remaining in the cells at $T = 30$ or 90 min was assessed by scintillation spectrometry. Percent efflux was calculated as the ratio (×100) of 5-HT efflux divided by 5-HT accumulated in parallel plates, not subjected to efflux, at $T = 0$. No difference was observed in % efflux for plates pre-loaded for 30 or 90 min (data not shown).

Total and Cell Surface Expression Protein Analysis—To determine total and surface expression of hSERT with wild type and/or mutant constructs, HeLa cells were plated in 24 or 12 well dishes at 100,000 or 500,000 cells per well, respectively, and transfected 18–24 h later as detailed above. Seventy two hours after transfection, cell surface proteins were biotinylated and

analyzed via Western blotting as described previously (28). Oocyte biotinylation experiments to quantitate surface expression of hSERT and hSERT mutants were performed as described previously (12) using 1.5 ng of cRNA and substituting EZ-Link Sulfo-NHS-biotin (Pierce) with EZ-Link Sulfo-NHS-SS-Biotin. Blots of total and surface protein were probed with ST-01 from Mab Technologies., Inc. (Stone Mountain, GA), and developed using Western Lightening Chemiluminescent Plus reagent (PerkinElmer Life Sciences).

Evaluation of Cysteine Accessibility—To probe for ion-dependent hSERT conformational movements, HeLa cells were plated on poly-D-lysine-coated 24-well TopCount plates at a density of 50,000 cells/well and transfected as described above. Twenty four hours post-transfection, cells were washed one time with 2 ml, one time with 1 ml, and one time with 500 μl of MKRH (MKRHG without glucose) $\pm$ 120 mM Cl^- and $\pm$ 50 μM 5-HT. Following a 5-min incubation, solutions were aspirated and replaced with 500 μl of 2 mM MTSET in MKRH. MKRH alone was added to one set of wells as a control. MTSET-treated wells were washed twice with 750 μl of MKRH followed by aspiration and addition of 225 μl of MKRHG. Cells were allowed to equilibrate to 37 °C for 10 min followed by addition of 25 μl of 200 nM [^{3}H]5-HT containing 10× ascorbic acid/HCl and iproniazid phosphate. After 10 min at 37 °C, wells were washed three times with 500 μl of ice-cold MKRH. MicroScint 20 (0.5 ml) was added to each well, and the accumulated 5-HT was quantified.

rSERT N101A/S404C accessibility was examined using MTSEA. HeLa cells were plated in 96-well plates at a density of 50,000 cells/well transfected and infected with vTF7-3 as described above. Twenty hours post-transfection, cells were washed three times with phosphate-buffered saline with magnesium and calcium (PBS: 137 mM NaCl or equimolar concentration of NMDG-Cl or sodium isethionate, 2.7 mM KCl, 4.3 mM Na_2HPO_4, and 1.4 mM KH_2PO_4, pH 7.3) containing 0.1 mM $CaCl_2$ and 1 mM $MgCl_2$ (PBSCM). Following a 5-min incubation, solutions were aspirated and replaced with 50 μl of MTSEA in the indicated concentrations in 50 μl of PBSCM. After 10 min, the cells were washed five times with 100 μl of PBSCM followed by incubation with 20 nM [^{3}H]5-HT for 10 min in 50 μl of PBSCM. After 10 min, wells were washed three times with 100 μl of PBSCM. Optifluor (PerkinElmer Life Sciences) (150 μl) was added to each well, and accumulated 5-HT was measured in a Wallac MicroBeta plate counter. Cells transfected with S404C was used as the control.

hSERT Expression in Xenopus laevis Oocytes—Oocytes were isolated, and cRNA was prepared as described previously (12, 30). cRNA was injected on the day of oocyte harvest. hSERT, N101A, N101C, S336C, N101A/S336C, and N101C/S336C cRNA were transcribed from NotI-linearized constructs in pOTV vector (a gift of Dr. Mark Sonders, Columbia University) using Ambion mMessage Machine T7 kit (Ambion, Austin, TX). Each oocyte was injected with 1.5 ng of cRNA and incubated at 18 °C for 4–6 days in Ringer's buffer (100 mM NaCl, 2 mM KCl, 5 mM $MgCl_2$, 5 mM HEPES, pH 7.4) supplemented with 550 μM/ml sodium pyruvate, 100 μg/ml streptomycin, 50 μg/ml tetracycline, and 5% dialyzed horse serum. Whole-cell currents were measured by two-electrode voltage clamp techniques using a GeneClamp 500 (Molecular Devices, Palo Alto, CA). Microelectrodes were pulled using a programmable puller (Model P-87, Sutter Instrument, Novato, CA) and filled with 3 M KCl (0.5–3-megohm resistance). A 16-bit A/D converter (Digidata 1322A, Molecular Devices) interfaced to a PC computer running Clampex 9 software (Molecular Devices) was used to control membrane voltage and to acquire data. To induce hSERT-associated current, oocytes were perfused with 5-HT (typically 5 μM) in buffer (120 NaCl mM, 5.4 mM potassium gluconate, 1.2 mM calcium gluconate, 7.2 mM HEPES, 0.1 mM iproniazid, pH 7.4) using a gravity flow system (4–5 ml/min). Buffer pH was adjusted with KOH or $KHPO_4$. The 5-HT-induced current was defined as current in the presence of 5-HT minus current in the absence of 5-HT. Substitution of Cl^- was performed as with the tissue culture studies above and are indicated in the text and figures. To minimize liquid junction potentials, Cl^- substitution experiments were performed using a 1 M KCl, 2% agar salt bridge to isolate the Ag-AgCl electrode from the bath. For constant voltage recordings, data were low pass filtered at 10 Hz and digitized at 20 Hz. For current-voltage (*I-V*) recordings, the voltage was changed stepwise every 500 ms. Currents were low pass filtered at 100 Hz and digitized at 200 Hz. All analyses were performed using Origin 7 (OriginLab, Northampton, MA) and GraphPad Prism (GraphPad software, San Diego).

Simultaneous Measurement of 5-HT Uptake and 5-HT-induced Currents—Simultaneous measurement of 5-HT uptake and 5-HT-induced current was performed under voltage clamp conditions, using techniques described previously (31). Oocytes were perfused for 150 s under voltage clamp with 1 μM [^{3}H]5-HT (specific activity = 3.12 Ci/mmol). To minimize loss of 5-HT, oocytes were perfused with ice-cold buffer for 250 s prior to removal from the chamber. The total charge movement was calculated by time integration of 5-HT-induced inward currents and related to the amount of 5-HT taken up in the same oocyte. Nonspecific 5-HT uptake was determined using water-injected control oocytes analyzed under the same conditions. Oocytes were solubilized with 200 μl of 0.1% SDS and 10 ml of EcoScint H (National Diagnostics, Atlanta, GA), and 5-HT accumulation was quantified by liquid scintillation spectrometry (Packard Instrument Co.).

hSERT Molecular Modeling—Molecular models for hSERT were generated using the template structure of $LeuT_{Aa}$ (PDB_ID 2A65) as detailed elsewhere (32). The binding mode for 5-HT identified as the one most consistent with available experimental data by Kaufmann *et al.* (32) was taken as the starting point for model refinement using the AMBER forcefield. Briefly, ions were added to the energy-minimized model of 5-HT in complex with hSERT to generate refined models that either contained NaCl or omitted Cl^- (Na^+ only). Two Na^+ ions were added to both the Na^+ (without Cl^-) and NaCl models by superimposing the hSERT model reported by Kaufmann *et al.* (32) with the x-ray structure of $LeuT_{Aa}$ and utilizing the coordinates of atom NA 752 (Na1-binding site) and NA 751 (Na2-binding site). For the NaCl model, a single Cl^- ion was centered on the region of the hSERT model occupied by the side-chain carboxyl group of residue Glu-290 in LeuTAa, as recently validated in studies of SERT and GAT (33, 34). Models

of the hSERT ion-binding sites were then refined with 50 steps of "steepest descents" and 450 steps of gradient-based minimization in AMBER9 (32) followed by brief (1 ns) low temperature (50 K) molecular dynamics simulations *in vacuo*, using a distance-dependent dielectric constant and 12-Å cutoff for nonbonded interactions to energetically relax the system. The resulting structures were then subjected to an additional round of energy minimization as described above to generate the reported models. Partial charges for 5-HT were ascribed using the atom-centered point charge method of Bayly and Kollman (35). All other molecular mechanics parameters for 5-HT and ions were taken from the standard AMBER force field with the exception of acetate. Acetate parameters were derived by analogy to the ionized form of the carboxylic acid side chain of aspartate from the standard AMBER9 database truncated at the CB atom with total partial charge equal to −1.0). Two-dimensional schematics of the refined hSERT ion-binding sites were generated with ChemDraw 10.0 (Cambridge Soft), and three-dimensional representations were rendered with PyMol (Schrödinger, LLC).

Molecular Dynamics and Free Energy Perturbation (FEP) Simulations—Molecular models of a protonated 5-HT were developed where the geometry parameters (bond lengths and angles) were obtained by quantum mechanics minimization at the B3LYP/6–31G* level of theory using the restrained electrostatic potential fitting approach described by Anisimov *et al.* (36). The net charge of 5-HT molecule was set to +1 with the side-chain nitrogen protonated based on the reported pK_a values. Parameters for deprotonated cysteine (thiolate ion) for pK_a computations have been validated and published before by Foloppe and Nillson (37). For equilibrium MD simulations, the starting configuration for SERT complexed with the 5-HT, two sodium, and one chloride ion was taken from the minimized molecular model described above. The S352C, S336C, and N101A mutants were obtained with a side-chain rotamer library search using SCWRL3.0 software (38). The complexes were next embedded into a lipid membrane using a multiple step membrane building procedure used in previous studies (39). The simulation box contains the 5-HT transporter, bound sodium ions with (or without) chloride/acetate ions, one serotonin substrate, and 204 1-palmitoyl-2-oleoylphosphatidylcholine lipid molecules solvated in an explicit 150 mM NaCl aqueous solution. All computations were carried out by NAMD version 2.7b1 (40), and analysis was done with CHARMM version c36b2 with the CHARMM27 force fields for proteins and lipids (41). MD simulation methods used here are similar to those used in previous studies of membrane systems (42, 43). Briefly, constant temperature/constant pressure algorithms were applied (with pressure at 1 atm and temperature at 315 K). Electrostatic interactions were treated with the Particle Mesh Ewald algorithm with a 104/104/96-Å grid for fast Fourier transform, $\kappa = 0.34$ Å^{-1}, and a 6th order spline interpolation. The nonbonded interactions were smoothly switched off at 12–14 Å. All simulation systems were equilibrated for 5 ns each without any constraints, and the production was run for another 15 ns. Further details on protocols used for FEP and molecular mechanics/Poisson-Boltzmann surface area simulations can be found in the supplemental materials.

RESULTS

hSERT Asn-101 Mutation Eliminates Cl^- Dependence of 5-HT Uptake—To examine a role of hSERT Asn-101 in the Cl^- dependence of 5-HT transport, we transfected HeLa cells with hSERT or hSERT N101A and N101C mutants and measured the effect of extracellular Cl^- on 5-HT transport saturation kinetics (Fig. 1). As described previously (44), removal of external Cl^- from the medium of hSERT-transfected cells resulted in a significant (5-fold) decrease in 5-HT transport V_{max} (NaCl, 0.068 ± 0.006 fmol/cell/min; sodium gluconate, 0.014 ± 0.002) and a significant (3.6-fold) increase in 5-HT K_m (NaCl, 0.9 ± 0.2 μM; sodium gluconate, 3.2 ± 0.36 μM, one-way ANOVA, Dunnett's post hoc, $p < 0.002$). Remarkably, the hSERT N101A and N101C mutants were largely insensitive to Cl^- substitution with gluconate (Fig. 1, *b* and *c*). Moreover, the 5-HT K_m values of N101A and N101C were not influenced by the presence of Cl^-, unlike hSERT, and were comparable with the 5-HT K_m values obtained for hSERT in the presence of Cl^- ($N101A_{+Cl}$ 1.45 ± 0.4 μM, $N101A_{-Cl}$ 1.66 ± 0.2 μM; $N101C_{+Cl}$ 1.20 ± 0.3 μM, $N101C_{-Cl}$ 1.4 ± 0.2 μM; $hSERT_{+Cl}$ 0.87 ± 0.2 μM, $hSERT_{-Cl}$ 3.2 ± 0.4 μM). The rate of 5-HT transport by hSERT was a monotonic function of extracellular Cl^- concentration (Hill = 0.8 ± 0.1) with an EC_{50} of 7.5 mM (Fig. 1*d*), in line with previous studies of rSERT (45). Across the same Cl^- concentration range, the N101C and N101A mutants exhibited virtually no further stimulation of 5-HT transport.

Asn-101 Dictates Cl^--dependent Conformational Changes in TM1 and EL4—Asn-101 could dictate the Cl^- sensitivity of hSERT simply by stabilizing binding of the anion. Alternatively, Asn-101 may be required to translate anion binding into critical conformational changes linked to the Na^+-coupled, 5-HT transport process. To examine these issues, we first examined the ability of Cl^- to alter aqueous exposure of three residues proposed to report steps in the transport cycle, Cys-109, Ser-404, and Ser-277 (Fig. 2). Each of these positions is distant from the 5-HT- and Cl^--binding sites, so changes in their accessibility are likely to reflect conformational changes because of ligand binding rather than direct binding itself. Cys-109 lies at the extracellular end of TM1 and is the major determinant of wild type SERT sensitivity to MTS reagents (Fig. 2) (46, 47). MTS-mediated inactivation of Cys-109 is sensitive to Na^+ replacement with Li^+ and is also modulated by 5-HT (46, 48), possibly a sign that this residue sits within a conformationally active domain that is mobilized by ion and neurotransmitter binding. We found that the presence of Cl^- significantly protected Cys-109 against inactivation by the positively charged MTSET (Fig. 3*a*), independent of the presence of 5-HT. In contrast, hSERT N101A was not protected against MTSET inactivation by Cl^-, consistent with the lack of Cl^- dependence measured for N101A in 5-HT transport assays (Fig. 1). That Cys-109 was the target for inactivation by MTSET in hSERT N101A, as opposed to another endogenous cysteine, we found that the C109A/N101A double mutant was insensitive to MTSET (data not shown). Strikingly, whereas 5-HT had little or no ability to protect wild type hSERT against MTSET inactivation in Cl^--free conditions, 5-HT provided significant protection to hSERT N101A (Fig. 3*a*) in the absence or presence of

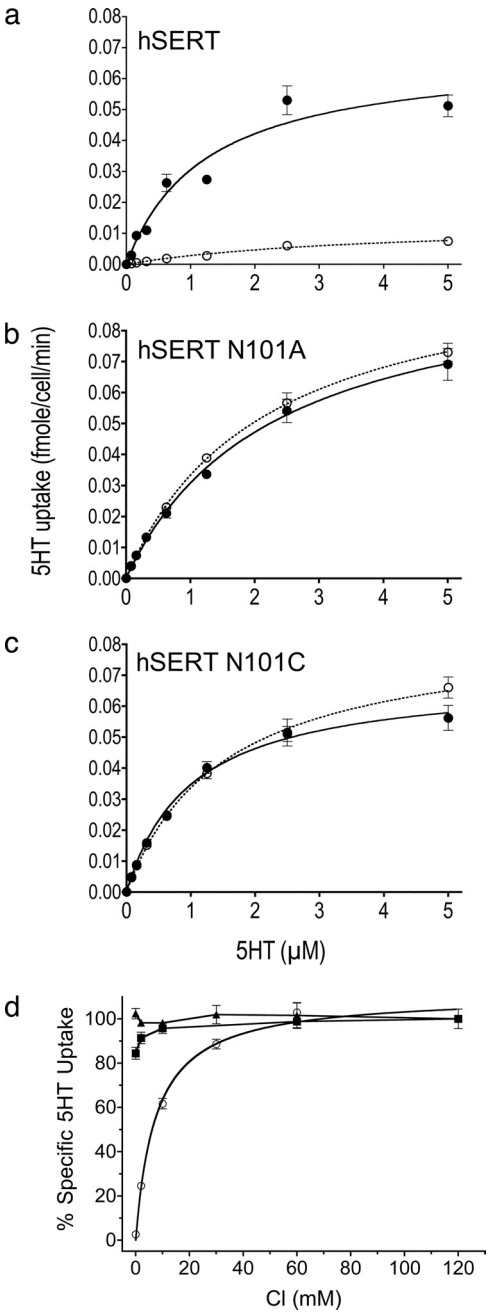

FIGURE 1. **Kinetic analysis and Cl^- dependence of 5-HT uptake in hSERT Asn-101 mutants.** HeLa cells transiently expressing the hSERT (*a*), hSERT N101A (*b*), or hSERT N101C (*c*) were evaluated for dose-dependent 5-HT uptake after 10 min in the presence (*solid line/filled circles*) or absence (*dashed line/open circles*) of Cl^-. *d*, dependence of 5-HT uptake on Cl^- concentration lost in Asn-101 mutants. HeLa cells transiently expressing hSERT (○), hSERT N101A(■), or N101C (▲) were incubated with increasing concentrations of Cl^- and assayed for uptake of [^{3}H]5-HT after 10 min. Remaining anion concentration was accounted for by addition of methanesulfonate. DNA amounts transfected were 200 ng/well for N101A and N101C and 25 ng/well for hSERT to account for differences in surface expression.

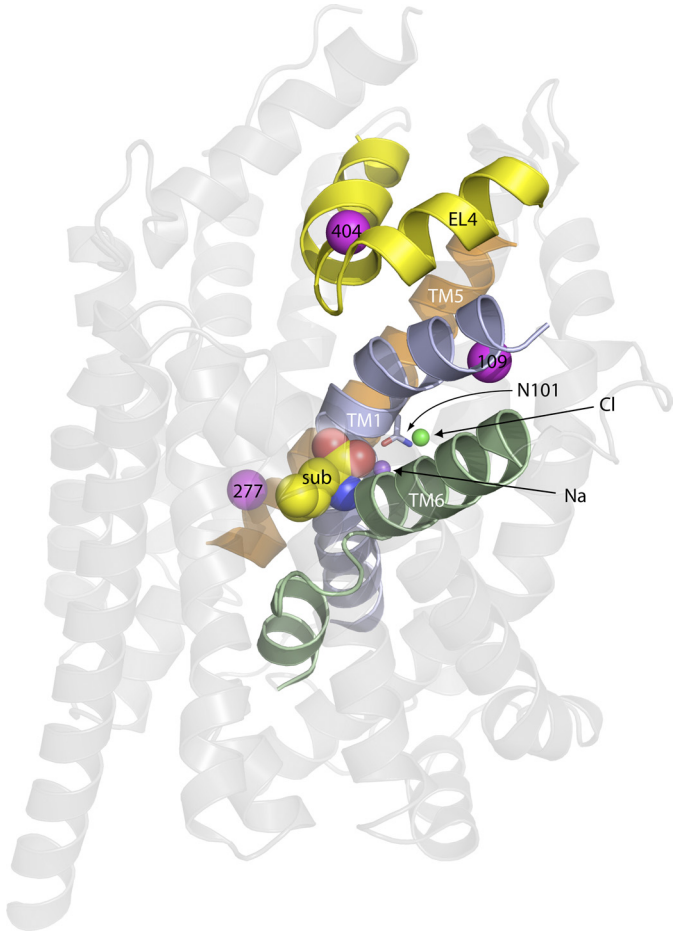

FIGURE 2. **Mapping of MTSET probes and Cl^--binding site from hSERT onto the LeuTAa crystal structure.** Illustration shows hSERT features discussed in this study as follows: 1) MTSET targeted cysteine mutants (*magenta spheres* numbered with the corresponding hSERT residue and their respective domains (TM1, *blue*; TM5, *orange*; EL4, *yellow*, and TM6, *green*); 2) space-filling model of substrate in the binding site (sub); 3) ions Na^+ and Cl^- (*purple* and *green spheres*, respectively); and 4) *stick* representation of the Asn-101 side chain.

the anion. These data suggest that Asn-101 is required to transduce Cl^- binding to allow 5-HT-dependent conformational changes that involve TM1 and associated elements, as reported by Cys-109 modification. In the Asn-101 mutants, 5-HT induced a similar conformational change, but this effect did not require the presence of Cl^-. Ser-404, located in the middle of EL4 (Fig. 2), has been proposed to report reorientation of another external component of the 5-HT permeation pathway (49). Unlike Cys-109 in hSERT, however, Cl^- substitution in the absence of 5-HT does not afford protection of S404C (in a C109A background) to the membrane-permeant MTSEA (Fig. 3*b*), although Cl^- and 5-HT together do induce protection. We found that, just as with Cys-109, the aqueous accessibility of S404C in an N101A background is sensitive to 5-HT in either Cl^--containing or Cl^--free medium. These studies confirm previous data (49) that transport-linked conformational changes in EL4 are associated with the loading of all three substrates and demonstrate that mutation of Asn-101 allows just 5-HT and Na^+ to trigger conformational changes in EL4. Cys-109 and Ser-404 are external reporters of conformational changes arising with substrate binding. In contrast, Ser-277 in TM5 (Fig. 2) is positioned to contribute to the cytoplasmic permeation pathway for 5-HT. Indeed, increased Ser-277 accessibility is believed to report an "open-to-in" conformation of the transporter (50, 51). Na^+ and Cl^- are required for the 5-HT-dependent exposure of residues in the cytoplasmic permeation pathway of SERT (50, 51). Fig. 3*c* demonstrates that 5-HT increases the extent of MTSEA inactivation in rSERT S277C

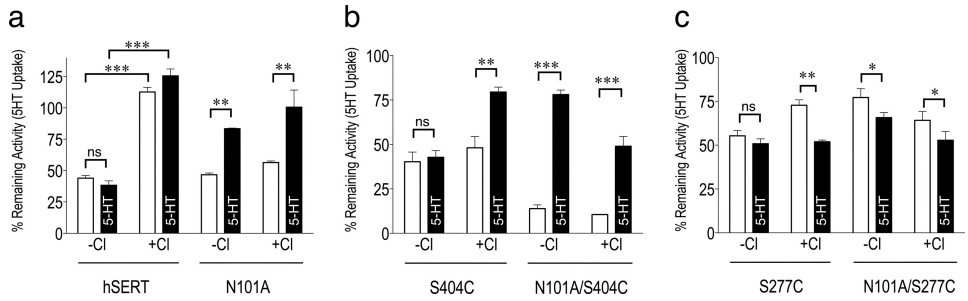

FIGURE 3. **Assessment of MTSET accessibility of targeted cysteines as a prediction of conformation change.** Tissue culture cells expressing hSERT or hSERT N101A (*a*), rSERT S404C or rSERT N101A/S404C (*b*), and rSERT S277C or rSERT N101A/S277C (*c*) were pretreated with MTSET in the absence (*open bars*) or presence (*black bars*) of 5-HT (50 μM) and in the absence or presence of Cl^- as indicated. Following treatment, 5-HT uptake assays were performed in normal uptake buffer to quantitate activity. Percent remaining activity is plotted and is defined as the amount of 5-HT uptake of MTSET- (*a*) or MTSEA (*b* and *c*)-treated cells as a percent of untreated cells. A two-tailed *t* test was performed on sample sets as indicated with brackets; *, $p < 0.05$; **, $p < 0.01$; ***, $p < 0.001$. *n.s.*, not significant.

only when Cl^- is present. In the N101A/S277C double mutant, however, 5-HT alone increased the extent of MTSEA inactivation demonstrating Cl^- independence. As the sensitization of S277C afforded by 5-HT in the N101A background still required the presence of Na^+ (data not shown), the cytoplasmic pathway appears to still be coupled to Na^+ with Asn-101 substitution, reinforcing a specificity for disruption of Cl^- coupling in Asn-101 mutants.

hSERT Asn-101 Dictates Ion Selectivity of 5-HT-independent Charge Flux—hSERT expressed in *X. laevis* oocytes (52) and mammalian cells (53) conducts both 5-HT-independent and -dependent currents, in addition to transporting 5-HT. Both 5-HT-independent ("leak current") and -dependent currents require extracellular Na^+ and Cl^- (54, 55), although it is unknown whether the 5-HT-dependent and -independent currents share a common pathway and/or molecular contacts as they permeate SERT. To assess whether mutation of Asn-101 removes the Cl^- dependence of SERT currents or affects stoichiometric charge movements, or both, we monitored hSERT-mediated currents in oocytes recorded under two-electrode voltage clamp. Prior to measuring currents, we determined the abundance of wild type and Asn-101 mutant hSERT expressed on the oocyte surface by biotinylation. Consistent with prior measurements of hSERT N101C surface expression in HeLa cells (28), whole-oocyte biotinylation studies revealed reduced cell surface expression of Asn-101 mutants (N101A and N101C, 61 ± 5.7 and 32 ± 8.7% of hSERT, respectively; Fig. 4*d*), although SERT-dependent transport and currents were readily detectable. In the oocyte biotinylation studies, a band was observed in the total (uninjected) control lane similar in size to mature hSERT. However, the band appears to be nonspecific as the same control lane lacks the immature and oligomeric hSERT bands observed in the hSERT-expressing oocytes, and this band is not observed in the surface control lane. As shown in Fig. 4*a*, 5-HT induced larger currents in Asn-101 mutants compared with wild type hSERT despite reduced surface expression. These currents were absent from mock-injected oocytes and were blocked by co-application of SERT antagonists (data not shown). Additionally, as first described by Mager *et al.* (56), antagonist (RTI-55) treatment of hSERT-expressing oocytes revealed a 5-HT-independent current that appears as an outward current at −60 mV (Fig. 4*a*) and that reverses at approximately +30 mV (Fig. 4*b*). The apparent outward current is interpreted as RTI-55 block of inward leak current. In contrast to 5-HT transport (56), the hSERT leak current was insensitive to extracellular Cl^-, except at high positive potentials where a slight reduction in maximal outward current was evident (Fig. 4*b*). These data indicate that Cl^- flux does not constitute a significant fraction of the 5-HT-independent current, consistent with the reversal potential of +30 mV. Like hSERT, the N101A mutant was insensitive to external Cl^-. However, in this mutant, the reversal potential for these currents (using RTI-55 to define the leak) shifted from approximately +30 to approximately +70 mV (Fig. 4*c*). The movement of ions during these experiments is insufficient to alter the internal ionic concentration of the oocyte, even less so in the presence of endogenous ion pumps. Thus, the shift in reversal potential we observe toward E_{Na} is most likely an inherent effect of the mutant on the ion selectivity of 5-HT independent currents. In support of this hypothesis, replacing all Na^+ with NMDG in normal Cl^- buffer shifts the hSERT reversal negative by 40.1 ± 3.8 mV, $p < 0.05$, $n = 7$, whereas N101A shifts by 52.6 ± 3.3 mV (S.E.), $p < 0.05$, $n = 6$. These changes are consistent with a shift toward a greater contribution of Na^+ to 5-HT independent currents in the N101A mutant than in hSERT.

Asn-101 Dictates Cl^- Dependence of 5-HT-induced Currents—Similar to leak currents, currents elicited by 5-HT were significantly larger in the Asn-101 mutants than in wild type hSERT when normalized for surface expression (Fig. 5*a*). Even more striking was the loss of Cl^- dependence for these currents in Asn-101 mutants (Fig. 5, *a–d*). In the hSERT N101C mutant, 5-HT actually induced slightly larger current (I_{max}) at negative potentials in the absence of Cl^- and current decreased in response to increasing Cl^- concentrations (Fig. 5*d*). These data can be explained if Cl^- is still transported through the N101C mutant, offsetting the Na^+ current. As described previously, 5-HT-induced currents in hSERT and rSERT did not reverse at positive potentials (52) because of outward leak currents that begin to dominate at positive potentials (Fig. 5*b*) (57). In contrast, a reversal of 5-HT-induced currents is evident at approximately +75 mV for both hSERT N101A and N101C. This finding is consistent with the loss of outward leak currents in the Asn-101 mutants at positive potentials (Fig. 5, *c* and *d*). Analysis of the Cl^- concentration dependence of 5-HT-induced currents (−60 mV, 5 μM 5-HT) confirms that although 5-HT-

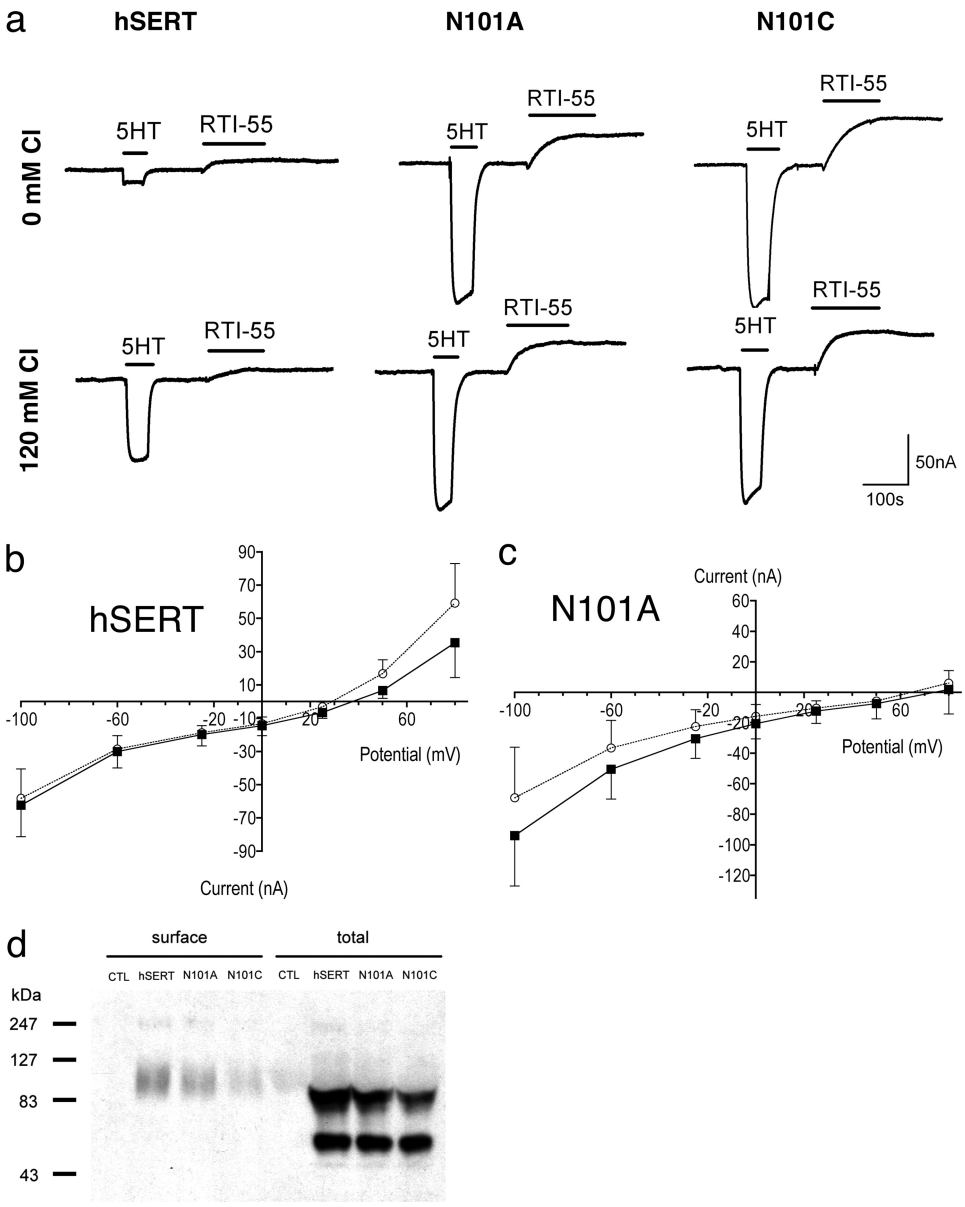

FIGURE 4. **Current-voltage relationship analysis of the hSERT leak conductance of N101A mutant.** *a,* current traces of 5-HT-induced (5 μM 5-HT) and leak current (revealed by application of the SERT antagonist RTI-55 (5 μM RTI-55)) from oocytes expressing hSERT mutants. Oocytes were injected with equimolar amounts of cRNA. Steady-state *I/V* analysis of leak currents for hSERT (*b*) and N101A (*c*) recorded in Ringer's buffer containing either 120 mM NaCl (○) or 120 mM sodium methanesulfonate (■). Values plotted represent the difference between conductance in buffer alone *versus* addition of 5 μM RTI-55. Because of the low levels of leak current observed in the hSERT-expressing oocytes compared with the Asn-101 mutants, only hSERT-expressing oocytes showing relatively higher leak currents were used to have sufficient signal for the *I/V* analysis. The traces in *a* reflect the average observed leak for hSERT and Asn-101 mutants. *d,* Western blot analysis of total and surface expression of hSERT detected with hSERT-specific monoclonal antibody ST-01. Equal amounts of protein were loaded in each lane. A band of similar size to mature hSERT was noted in the total (uninjected) control lane. However, the band is nonspecific as the total control lane lacks the immature and oligomeric hSERT bands observed in the hSERT-expressing oocytes, and no bands are observed in the surface control (*CTL*) lane.

activated current in hSERT required Cl^- (EC_{50} = 0.5 mM), Asn-101 mutants did not require Cl^- over the same concentration range (Fig. 5*e*). Unlike the shifted K_m value for 5-HT transport in the absence of Cl^- (Fig. 1*a*), the EC_{50} values for 5-HT-elicited currents in hSERT were unaffected by external Cl^- (1.6 *versus* 1.8 μM, respectively) (Fig. 5*f*). The 5-HT EC_{50} values for N101A and N101C were also Cl^--insensitive but were significantly decreased relative to hSERT values ($N101A_{-Cl}$ 0.78 ± 0.14 μM, $N101A_{+Cl}$ 0.64 ± 0.11 μM; $N101C_{-Cl}$ 0.72 ± 0.13 μM, $N101C_{+Cl}$ 0.39 ± 0.05 μM, $p < 0.05$ one-way ANOVA, Dunnett's post hoc test) consistent with the lower K_m value for 5-HT measured in the mutants (Fig. 1).

Asn-101 Dictates hSERT Coupling and Stoichiometry—To investigate the larger 5-HT-induced currents exhibited by the Asn-101 mutants, we determined 5-HT flux and total charge movements in hSERT and hSERT Asn-101 mutants in single voltage-clamped (−600-mV) oocytes (12). As shown in Fig. 6*a*, in normal extracellular Cl^-, hSERT supported the net inward movement of ~7 positive charges per 5-HT molecule, consistent with previous studies (10, 56). Removal of Cl^- caused a modest but significant increase in the flux ratio (~10 charges/5-HT), arising from a relative retention of 5-HT-gated currents despite a reduction in 5-HT transport. Charge/5-HT flux ratios in the Asn-101 mutants were significantly greater than for

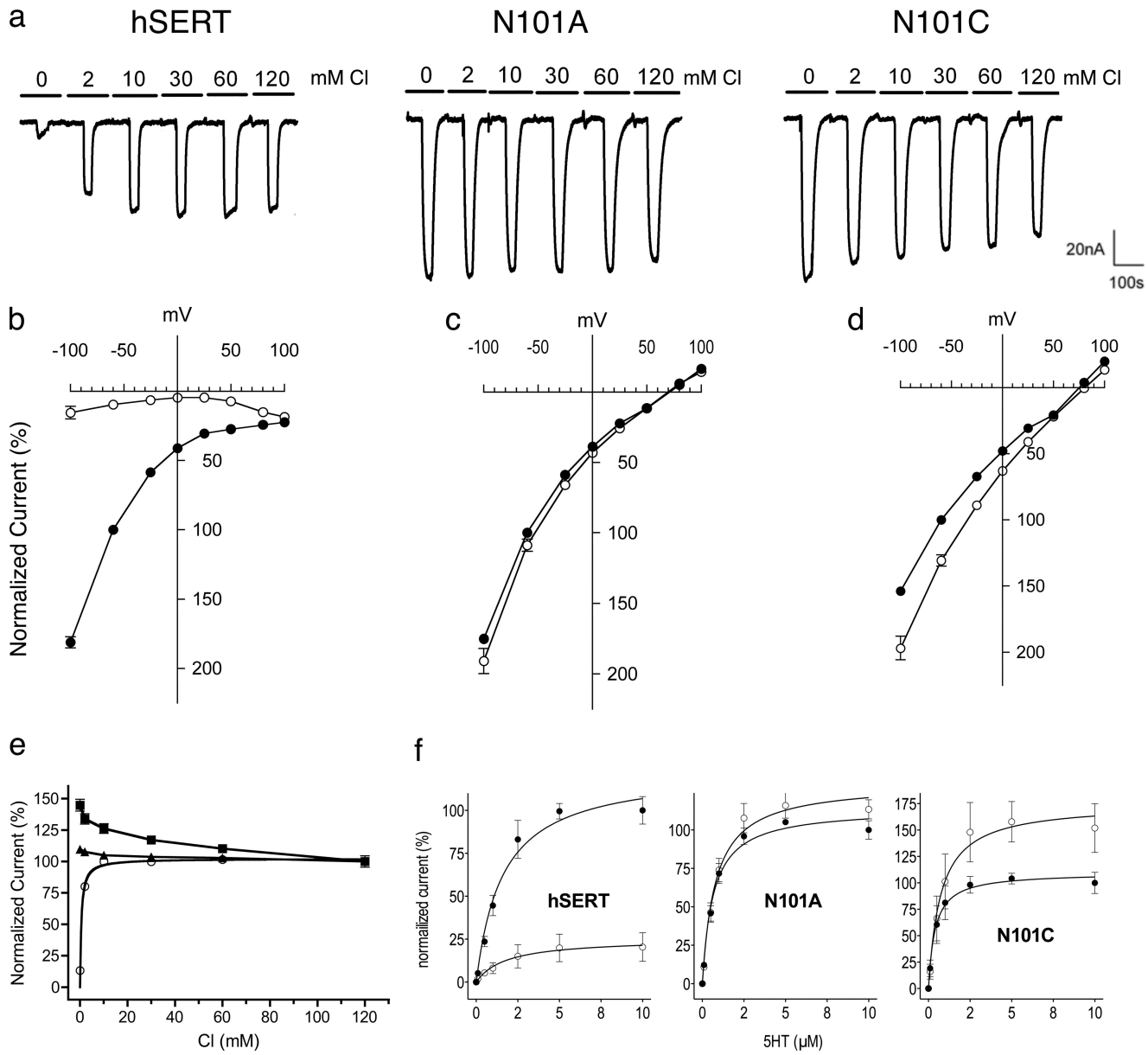

FIGURE 5. **TEVC analysis of Asn-101 mutants.** Dependence of $I_{5\text{-HT}}$ on Cl^- concentration. *a,* raw traces of Cl^- dose-dependent 5-HT-induced currents (5-HT, 5 μM). Cl^- addition is designated by *bars* along with concentration used. Anion concentration was adjusted with 120 mM with MS. Current-voltage relationship for the 5-HT-induced current reveals a reversal equilibrium for Asn-101 mutants. Steady-state currents evoked upon application of 5 μM 5-HT in the presence (●) or absence (○) of Cl^- and normalized to % current obtained with 120 mM Cl^- at −60 mV are plotted in relation to membrane potential for hSERT (*b*), N101A (*c*), and N101C (*d*). *e,* plot of induced current amplitudes from hSERT (○), N101A (▲), and N101C (■) from *a*. Currents were normalized to current obtained at 120 mM Cl^-. Cl^- was replaced with 120 mM methane sulfonate. *f,* plot of induced current as a function of 5-HT concentration in the presence (●) or absence (○) of Cl^- and normalized to percent current at saturation conditions in the presence of Cl^-. Cl^- was replaced with 120 mM MS.

hSERT, in the presence or absence of Cl^-, with ~40 charges moved per 5-HT. When normalized for transporter surface expression, this dramatic increase in the charge/5-HT flux ratio resulted from increased charge movement (rather than a reduction in 5-HT transport; data not shown), suggesting a disruption of coupling between transmembrane flux of Na^+ (or other ions) and 5-HT. To test this idea, we returned to mammalian cells where the smaller internal volume facilitates an assessment of equilibrium accumulation of 5-HT. After 2 h of incubation in 50 nM 5-HT, hSERT-transfected HeLa cells established a 281-fold (±14) gradient of $5\text{-HT}_{in}/5\text{-HT}_{out}$ (Fig. 6*b*). In contrast, the Asn-101 mutants concentrated 5-HT to a significantly lesser extent (N101A, 18-fold (±1); N101C, 31-fold (±1); $p < 0.01$, one-way ANOVA and Dunnett's post hoc analysis). Removal of the Cl^- gradient as a driving force in platelet plasma membrane vesicles led to a much smaller (~50%) decrease in 5-HT accumulation (58), consistent with an important role for Asn-101 in optimal coupling of 5-HT transport to the Na^+ gradient. Moreover, when transfected cells with accumulated 5-HT were washed and then incubated in 5-HT-free medium, hSERT Asn-101 mutant cells exhibited significantly more efflux of 5-HT (hSERT 31 ± 1.3% in 30 min; N101A 76 ± 1.7% ($p < 0.001$); N101C 71 ± 1.1% ($p < 0.001$, one-way ANOVA and Dunnett's post hoc analysis) (Fig. 6*c* and supplemental Fig. S9). Together, these data reveal that mutation of Asn-101 disrupts the ability of hSERT to utilize energy stored in transmem-

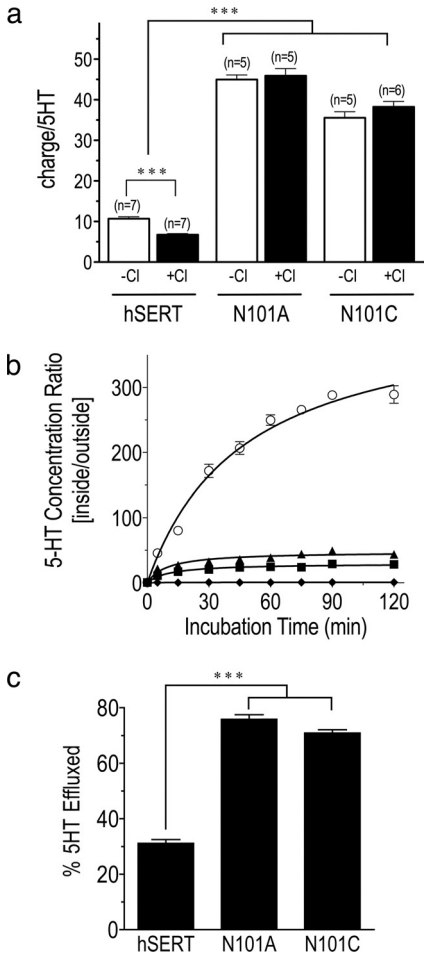

FIGURE 6. **Ion-substrate coupling analysis of hSERT Asn-101 mutants.** *a,* TEVC analysis of charge to substrate flux ratio. TEVC oocytes expressing hSERT or the Asn-101 mutants were exposed to [^{3}H]5-HT in the presence or absence of Cl^-. Induced current was monitored during the incubation period followed by quantitation of total 5-HT incorporated. Total current was converted to charge. The net charge movement per 5-HT molecule translocated was plotted for both presence (*filled bars*) and absence (*open bars*) of Cl^-. (***, $p < 0.001$). *b,* steady-state uptake kinetics. [^{3}H]5-HT (20 nM) uptake in NaCl-containing assay buffer by HeLa cells transiently transfected with hSERT (○), N101A (▲), N101C (■) or nontransfected (♦) is monitored over 120 min. Data are normalized by calculating the concentration ratio of [^{3}H]5-HT inside the cell compared with the concentration in the buffer. The data were fit to a Michaelis-Menten nonlinear regression equation. *c,* substrate efflux from cells preloaded with [^{3}H]5-HT. HeLa cells transiently transfected with hSERT, N101A, or N101C are incubated with 20 nM [^{3}H]5-HT for 30 min washed and allowed to efflux for 30 min in MKRH buffer. % [^{3}H]5-HT efflux is plotted and determined by comparing [^{3}H]5-HT remaining in the cells from efflux assay to duplicate samples halted prior to the efflux step. (***, $p < 0.001$).

brane ion gradients to support the intracellular accumulation of 5-HT.

Molecular Modeling Suggests a Mechanism for Asn-101 Participation in Ion-coupled 5-HT Transport—The lack of evidence for direct interaction between Asn-101 and Cl^- (33, 34, 59, 60) suggests that Asn-101 effects derive not from Cl^- binding. We investigated the possibility that Asn-101 served an essential role in propagating Cl^- binding at nearby sites to other critical determinants of 5-HT transport using Rosetta-Ligand (61) to dock 5-HT into an hSERT homology model and performed relaxation and energy minimization *in vacuo* with AMBER (32). Subsequently, models of wild type hSERT and the N101A mutant were evaluated both in the absence and in the presence of the Cl^- and acetate ions using the same protocol. The placement of 5-HT in our model is consistent with biochemical data that indicate coordination of the 5-HT amine by Asp-98 as well as sensitivity of 5-HT to substitution at various positions around the indole ring (62, 63). In hSERT, with Na^+, Cl^-, and 5-HT bound, our depiction illustrates these three substrates co-localized around the Na1 binding pocket through their coordination by residues of TM1, -2, -6, and -7 (supplemental Table S3). These four helices have been proposed to form a bundle whose movement within the protein closes the extracellular permeation pathway and opens a pathway to the cytoplasm (50). Our minimized structures also predict that Cl^- and Na^+ coordination is linked via dual interacting residues Ser-336 (TM6) and Asn-368 (TM7). 5-HT engages both the Na^+ and Cl^- coordination networks via a salt bridge provided by its ethylamine nitrogen. Asn-101 participates in Cl^- interactions in these models through stabilization of Asn-368 in TM7 and Na1. To test predictions from the gas-phase computations, we constructed a solvated lipid membrane system with our SERT models and performed all-atom MD simulations with the CHARMM-27 force field (supplemental Fig. S7).

Using different methods (comparative modeling, docking, minimization, and then all-atom MD simulations), we consistently observed distinct backbone conformational shifts at residue Ser-336 in response to Cl^- removal (Fig. 7, *a* and *b* and *d* and *e*) that result in a shift of hydrogen-bonding interactions of the Ser-336 side-chain OH away from interaction with the Asn-368 side-chain amide (Fig. 7, *a* and *d*), where many residue contacts in TM1, -2, -6, and -7 are affected, including Tyr-121 and Ser-372. The multiple interactions of Asn-101 observed in hSERT are likely critical to coupling as they lead to an extensive hydrogen bond and coordination network around the bound ion substrates. Conversely, Cl^- coordination of Asn-368 permits an interaction of the Ser-336 side-chain OH with Asn-368 via an improved geometry for coordination of the Na1 site Na^+ ion. In turn, these interactions link TM2 and TM7 to TM1, where critical aspects of 5-HT coordination are located (residue Asp-98 and the backbone carbonyl of Tyr-95) (Fig. 7, *a* and *d*). Notably, our recent substituted cysteine accessibility method analysis of TM6 (64) revealed S336C exhibits the same phenotype as the N101C mutant in that it is sensitive to +-charged MTS reagents and insensitive to −-charged MTS reagents.

Importantly, analysis of MD trajectories allow us to predict the residue interaction changes likely to arise in Asn-101 mutants that allow for Cl^--independent 5-HT transport. Analysis of the inter-residue contacts from MD simulations predicted that the N101A mutation can considerably disrupt the H-bond interaction network found in the hSERT substrate-Na1 ion-binding pocket (supplemental Table S3 and supplemental Fig. S8). Coordination of Na^+ by the Asn-101 side-chain amide oxygen is predicted to be lost as is the H-bond between 5-HT and Ser-336. A number of long lived (stable) bonds connecting TM2 and -7 are also lost in the hSERT WT sodium only models (Fig. 7, *b* and *e,* and supplemental materials). However, the Ala-101 side chain, being considerably smaller than Asn-101, permits a local repacking of the residues forming the Na1-binding

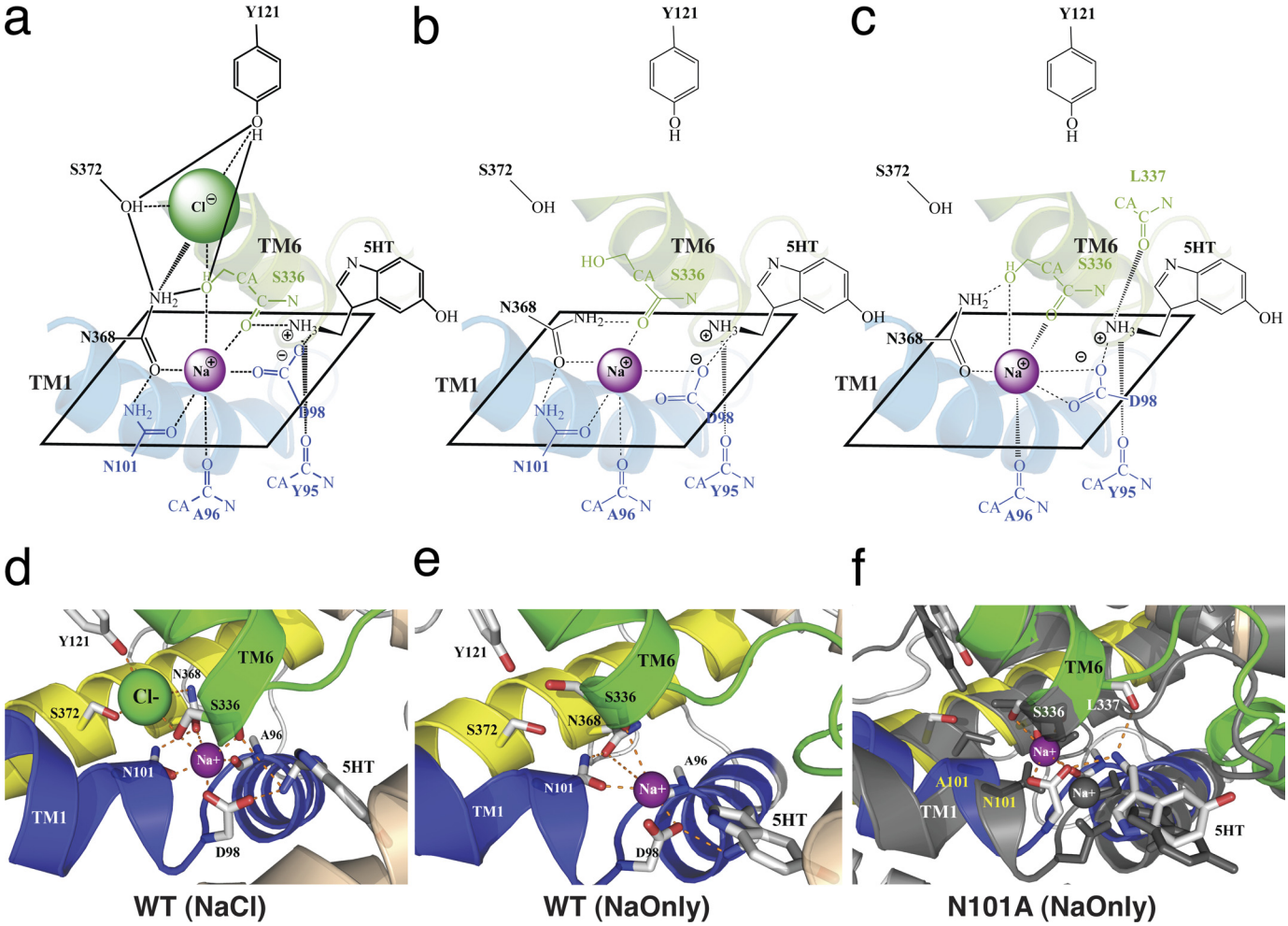

FIGURE 7. **Molecular models of putative hSERT ion-binding sites.** The *top panels* are 2.5-dimensional representations emphasizing differences in ion coordination geometry observed after a 20-ns MD simulation of our models. Residues participating in the ion-binding site of each model are color coded *blue* (TM1), *green* (TM6), and *yellow* (TM7) according to transmembrane helix. Note the apparent importance of residue Ser-336 in stabilization of favorable ion-coordination geometry in both the models for WT NaCl (*a*) and N101A mutant sodium only (*c*) hSERT models. *a,* WT hSERT *NaCl* model; *b,* WT hSERT *NaOnly* model; *c,* N101A mutant hSERT *NaOnly* model; *d,* three-dimensional rendering of WT *NaCl* hSERT model (2.5-dimensional in *a*); *e,* 3-dimensional rendering of WT *NaOnly* hSERT model (2.5-dimensional in *b*). *f,* 3-dimensional rendering of N101A mutant hSERT *NaOnly* model (color; 2.5-dimensional in *c*) superimposed on WT *NaOnly* hSERT model (*black*). All *dashed lines* represent stable hydrogen bonds observed after 20 ns of MD simulation in lipid membrane and aqueous solution, except ion coordination lines around shaded Na^+ (*purple*) and Cl^- (*green*) ions. Our relaxed models predict that stabilization of the "chloride-independent" phenotype in N101A mutant hSERT may involve coordination of sodium by the backbone carbonyl of Leu-337. *CA* in *a*–*c* = α-carbon. Na^+ was also placed in the Na2 site during MD analysis but is not displayed in the contact diagram here.

site and displacement of the Na^+ ion by ~2.0 Å (Fig. 7*f*, *gray* and *magenta spheres*). This change allows formation of a novel Na^+ coordination site in which the backbone carbonyl of Ser-336 supplements the Ser-336 side chain, restoring WT-like ion coordination number ($n = 6$) with the backbone carbonyl of Leu-337 (TM6) forming an H-bond with the 5-HT ethylamine moiety. Interestingly, a conservative but bulkier N101Q mutation results in almost complete loss of function (data not shown) suggesting side chains larger than Asn may significantly impact interactions in the binding site. The Na1 site is further stabilized by Ser-336 forming an H-bond to the side chain of the Asn-368 amide. There is also a long living hydrogen bond (>80% of all analyzed MD frames) between Tyr-121 and Ser-372 (TM6). These interactions effectively mimic the relative positioning of the same residues from TM7/TM2/TM6/TM1 found in the WT hSERT Cl^- ion coordination models (Fig. 7, *a* and *d* and *e* and *f*).

Effect of Cl^- and Different Mutations on Ion and Solute Binding to the Transporter—To better understand the role of Cl^- in binding of Na^+ and 5-HT, we computed binding enthalpies using MM/PBSA approximation (65). The evaluation of binding enthalpies for mutants (101A and 336C) may help highlight the role of the anion in the transport cycle and its modulation by Asn-101 and Ser-336. The results from binding computations are summarized in supplemental Table S4. The $\Delta\Delta H$ for the Cl^--free WT protein shows significant inhibition of both Na^+ and 5-HT binding to the transporter indicating an important role of Cl^- in the stabilization of the entire binding pocket. The analysis of the ion coordination within the Na1 site shows that the anion-depleted transporter displays different ion coordination for Na1 than the anion-bound complex. In particular, the hydroxyl oxygen from the side chain of Ser-336 no longer coordinates the Na^+ ion, and the Na1 coordination number is reduced from ~6 to ~5 ligands producing an immediate effect

on ion binding affinity to Na1. In contrast, removal of Cl^- from the N101A mutant led to relatively modest changes in the binding enthalpies for solute and ions to the Na1/Na2 sites as compared with WT. In the N101A system, both side-chain carboxylate oxygens of Asp-98 and the side-chain OH and backbone carbonyl oxygen of Ser-336 are now participating in the coordination shell for the Na^+ ion bound to the Na1 site thereby compensating for the substitution at Asn-101 (Fig. 7*f*). Ser-336 contributes both main chain and side-chain oxygens to ion coordination in the N101A mutant (with and without Cl^- bound). However, binding of Cl^- to the N101A mutant destabilizes ion coordination at the Na2 site such that the affinity of Cl^- for the transporter is reduced relative to that of a wild type transporter. Thermodynamic analysis of binding enthalpies suggest that Asn-101 plays an important role in modulation of binding affinity at the Na1 and Na2 sites as well as a contribution to the modulation of Cl^- binding.

Validation of a Critical Partnership between Asn-101 and Ser-336 in Cl^--dependent 5-HT Transport—As noted above, our models suggest a critical relationship between Asn-101 in TM1 and Ser-336 in TM6 on the coupling of Na^+ and Cl^- binding to 5-HT transport. To test this hypothesis, we generated the Cys substitution S336C, reducing the length of the side-chain hydrogen bond donor because our model proposes that this side chain directly coordinates Cl^- as well as Asn-368 (Fig. 7*a*) (22, 34). Indeed, although surface expression of hSERT S336C was 70% of hSERT (supplemental Fig. S6*d*), transport activity was only 11 ± 2.7% (n = 3) that of wild type. Importantly, the residual 5-HT transport activity observed with S336C was largely Cl^--independent and was actually enhanced by full anion replacement with acetate (supplemental Fig. S6, *a*–*c*).

The findings with S336C are similar to results obtained by Forrest *et al.* (34) who proposed Ser-372 was a Cl^--coordinating residue in SERT (Fig. 7*a*) and found that mutation of Ser-372 to the negatively charged Asp or Glu yielded Cl^- independence. However, unlike N101C, S372C did not result in Cl^--independent uptake but rather yielded an increase in the apparent K_m value for Cl^-. This difference in Cys substitution at these two sites in terms of Cl^- independence could be explained by the pK_a at Ser-336 and Ser-372 in the absence of Cl^-. Cys-372 is proposed to be in the noncharged SH form (34). We constructed equilibrated and minimized hSERT models in a solvated membrane system and used free energy perturbation FEP analysis using dual topology methods (66) to evaluate pK_a shift upon deprotonation for cysteines at the positions 336 and 372 relative to model solution (150 mM aqueous solution of NaCl). FEP simulations of the pK_a shift for buried cysteines. These analyses reveal that in the presence of Na^+ in the Na1 site, Cys-336 can be deprotonated at pH 7 with a large ΔpK_a shift of approximately −5.0. The experimental pK_a for the Cys side chain is ~8.0, and therefore the pK_a for Cys-336 is ~3.0, suggesting that there is a high probability that the side chain of Cys-336 is deprotonated with Na^+ present at the Na1 site. However, analysis of Cys-372 shows the resulting ΔpK_a shift is approximately −0.9 and the net pK_a for Cys-372 is ~7.1. The reason for the apparent difference in protonation state at these two positions lies in the proximity to bound Na^+. MD simulations with $Cys\text{-}336^-$ show that the negatively charged side chain partially occupies the site for Cl^- and could coordinate Na^+ (with occupancy of ~40%). Cys-372 cannot coordinate to the positive ion, and therefore its deprotonation in the low dielectric environment is energetically unfavorable. These findings are consistent with the proposition that Cys-336 acts similar to charge-changing (Asp or Glu) mutations at the position 372 in providing a localized negative charge and thereby results in Cl^- independence. Whereas the convergence of free energy simulations is known to be a bottleneck of the method, large shifts in pK_a values are suggestive of different propensities in the protonation states of these two cysteines (67).

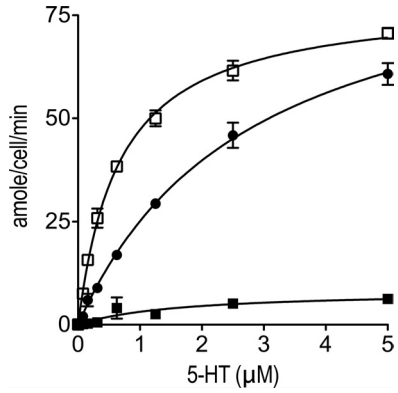

FIGURE 8. **Kinetic analysis of 5-HT transport in hSERT S336C and N101A/S336C mutants.** HeLa cells transiently expressing the hSERT N101A (□), hSERT S336C (■), or hSERT N101A/S336C (●) mutants were evaluated for dose-dependent 5-HT uptake after 10 min in 120 mM Cl^-, n = 3.

Interestingly, whereas in tissue culture studies S336C transported 5-HT at only ~11% the rate of wild type hSERT, introduction of N101A into the S336C background transport rate was three times faster, similar to that of the N101A single mutant alone (Fig. 8) (28). Like the Asn-101 and Ser-336 single mutants, 5-HT transport by the N101A/S336C and N101C/S336C double mutants is Cl^--independent (supplemental Figs. S5 and S6). Side-chain rotomer modeling of S336C in both wild type and N101A mutant backgrounds suggest steric packing effects in the Na1 ion-binding site were significant structural factors contributing to this phenotype (supplemental Fig. S1). Consistent with [^{3}H]5-HT transport assays, TEVC analysis of S336C single and N101A/S336C and N101C/S336C double mutants yields results similar to N101A and N101C mutants, where 5-HT-induced currents are Cl^--independent (supplemental Fig. S6*e*). As with the N101C single mutant (Fig. 5*e*), the N101C/S336C mutant shows a dose-dependent reduction in observed current in response to increasing Cl^- concentration suggesting the possibility of Cl^- co-transport in the N101C-containing mutant that could offset the movement of positive (Na^+) ions, appearing as a reduction in current.

DISCUSSION

In our previous biochemical analysis of hSERT TM1, we suggested that the conserved residue Asn-101 was proximal to the substrate- and cocaine-binding sites (28). A position proximal to the substrate-binding site was later substantiated by the LeuT crystal structure (22) and in relation to the competitive antagonist cocaine by subsequent LeuT model-guided studies

of dopamine transporter (68). Interestingly, during the substituted cysteine accessibility method analysis, we found N101C could be modified by the positively charged reagent MTSET but not by the negatively charged MTSES (28). This distinction does not reflect a direct antagonism of MTSES by Cl^- as Asn-101 is not likely to be directly involved in Cl^- binding (34, 59, 60). In fact, Cl^--free conditions fail to promote MTSES inactivation of the N101C transporter.[7] The inability of MTSES to inactivate the N101C mutant may arise from repulsion by the transmembrane dipoles that are predicted to exist at the central unwound regions in TM1 and -6 (69). Moreover, four recent reports that identify Cl^--binding sites and the coordinating residues in SERT and GAT1 do not implicate Asn-101 in this role (33, 34, 59, 60).

In this study, we provide several lines of evidence regarding a critical role that Asn-101 plays in coupling Cl^- binding to the conformational changes that are essential for Na^+-coupled 5-HT transport. In particular, our substituted cysteine accessibility method analysis reveals that the Asn-101 mutants no longer require Cl^- for 5-HT-induced conformational changes, providing more specific evidence for the involvement of Asn-101 in Cl^- dependence. The Asn-101 mutations increase nonstoichiometric charge movements carried by hSERT, both in the presence and the absence of 5-HT, indicating uncoupled ion movements. Conversely, although Asn-101 mutants transported 5-HT at initial rates comparable with that of hSERT, steady-state 5-HT accumulation was reduced ~90%, further indicating a loss of thermodynamic coupling between transmembrane gradients of ions and 5-HT. This loss of coupling was even more severe than would be expected simply from the contribution of a transmembrane Cl^- gradient to 5-HT accumulation, which was less than 2-fold in measurements with resealed vesicles expressing native SERT (58), suggesting a more profound defect in ion coupling in the Asn-101 mutants.

Slight differences in the extent of Cl^- substitution by the anions acetate (105%), methanesulfonate (78%), and gluconate (70%) correlate with their Stokes diameters of 4.5, 5, and 6.2 Å, respectively (supplemental Figs. S5 and S6), and suggest that Asn-101 substitution may impart changes in anion selectivity at the Cl^--binding site in SERT. These results indicate that anions may still interact with hSERT in the Asn-101 mutants and are consistent with the presence of all previously proposed Cl^--binding site residues (33, 34) in these mutants. Further evidence comes from Cl^- substitution with multivalent anions such as phosphate, resulting in poor functional replacement compared with monovalent species (≤40% compared with Cl^--containing conditions, data not shown). These data also suggest that the anion-binding site is still available, and its functional role can be inhibited by multiple charged species. The Asn-101/Ser-336 double mutants appear less sensitive to the anion size in replacement of Cl^- (supplemental Fig. S6, *b* and *c*) and Cl^- substitution.

Further insight into the role of Asn-101 and the impact of Asn-101 substitutions derives from our MD simulations. We utilized homology-based molecular modeling of hSERT using the $LeuT_{Aa}$ coordinates as well as small molecule docking of 5-HT with RosettaLigand. The results predict that Asn-101 extends into the substrate binding pocket where the side-chain carbonyl oxygen, homologous to $LeuT_{Aa}$ Asn-27 (22, 32), as proposed previously (22, 45), places Asn-101 in a critical position to contribute to the stabilization of both Na^+- and 5-HT-binding sites. Consistent with these findings, a docking study by Celik *et al.* (70) identified a similar pose for 5-HT in SERT as one of the three top-scoring clusters.

Ion and substrate dynamics are controlled by occupancy of Na1 and Cl^- sites. The mutations that affect ion binding to either site (Ser-336 or Asn-101) have a global impact on the entire transport mechanism. For example, our MD analysis implicated Ser-336 as an important residue in the Cl^- dependence of transport coupling. This residue was previously proposed to coordinate Cl^- in SERT (34, 60) and GAT-1 (33, 59), and we found that S336C exhibits the same insensitivity to MTSES as N101C (64). Experimental analysis of the hSERT S336C mutant subsequently revealed that like in N101C, 5-HT transport by S336C was not dramatically stimulated by Cl^-. However, our MD pK_a analysis suggests that this effect may also be due to replacement of Cl^- by the Cys thiolate anion, similar to replacement of other Cl^--coordinating residues with carboxylic amino acids in SERT and GAT-1 (33, 34). Finally, analysis of docking conformations indicates that the coordination geometry of acetate in the wild type is less favorable than in N101A and can explain why acetate can fully replace Cl^- in an Asn-101 mutant background but not in hSERT. In hSERT, acetate forms an H-bond with the C=O backbone of Ser-336 that would limit adoption of a Cl^--like geometry (supplemental Fig. S4, *a*, *c*, *d* and *f*). In N101A, the Asn-368 amide side chain is no longer constrained by the H-bond network imposed by Asn-101 and is thus free to interact with acetate in a manner that reproduces the ion coordination geometry of the WT NaCl model (supplemental Fig. S4, *b* and *e*).

More generally, our findings illustrate that both the direct interaction of Asn-101 with Asn-368 and the more indirect interaction with Ser-336 via coordination of the NA1 sodium ion suggest that establishment of physical interactions between TM1 and -6 is a critical facet of ion-coupled substrate movement. This idea is further supported and expanded by our inter-helical interaction energy analysis conducted on MD trajectories for WT and mutants (see supplemental material), which suggests that Cl^- removal has an adverse impact on transport by disruption of interactions between TM1 and -3, TM1 and -6, and TM5 and -8. In contrast, the removal of Cl^- is energetically much less disruptive to inter-helical interactions in the Asn-101 mutants. Recent crystal structure and MD studies suggest that the primary transport mechanism for the LeuT structural superfamily involves helical bundles that move relative to one another to allow entry to and exit from the substrate- and ion-binding sites (24, 50, 71, 72) via gating residues originally described by Yamashita *et al.* (22). However, there do exist disagreements between the models, and these differences may reflect mechanistic subtleties between transporters influenced by the substrates and ions involved.

Within the SLC6 family, some bacterial, insect, and mammalian family members differ in the identity of the residue homol-

[7] L. K. Henry and R. D. Blakely, unpublished observations.

ogous to hSERT Asn-101 and contain instead a His, Ala, Cys, Gly, Thr, Ser, or Asp (supplemental Fig. S2 and supplemental Table S2) (73), whereas all known Cl^--dependent SLC6 neurotransmitter transporters contain Asn at this site. This observation suggests that this residue bears a critical role in promoting optimal coordination of sodium, Cl^-, and substrate while limiting movement of additional charges, a role that appears relaxed in the Asn-101 mutants. As we and others (10, 14, 15, 17) have published that serotonin and dopamine transporter charge flux is an important contributor to neuronal excitability, we believe that the charge flux-limiting property of this residue is particularly important at synapses.

Neurotransmitter transporters are now known to exist in regulated protein complexes that can modulate multiple aspects of transport, including substrate affinity, membrane trafficking, and ion conductance states. Our observation of a >7-fold increase in Na^+ flux in the Asn-101 mutants and the finding that syntaxin 1a interaction with the N terminus of SERT can modulate Na^+ stoichiometry during the transport cycle (10) raise the possibility that syntaxin 1a binding may modulate transporter conductance states by orienting residues in TM1, likely including Asn-101, to restrict nonstoichiometric ion flow during the transport cycle. Although Ala (or Cys) can functionally replace Asn-101, the loss of optimal coupling is accompanied by dramatic increases in both leak and 5-HT-gated currents, properties that may be captured by syntaxin 1A-linked regulatory mechanisms. The remarkable >2-fold increase in 5-HT efflux from cells expressing the Asn-101 mutants also supports the idea that precise orientation of the amide side chain of this residue can control coupling between ion gradients and efflux of intracellular 5-HT. In fact, initial cation replacement studies using NMDG-Cl suggests that Na^+ dependence may be altered in the Asn-101 mutants (supplemental Fig. S3). In addition, it has been shown that amphetamine-induced efflux through dopamine transporter requires phosphorylation of its cytosolic N terminus (74) as a result of CaMKII activation by amphetamine. Phosphorylation of the N terminus may propagate changes in structure upward to TM1, recapitulating the impact of Asn-101 mutants. Finally, high NE flux rates mediated by channel-like states have been identified in the norepinephrine transporter (75). As these conductance states can be inhibited by syntaxin 1a (76), we speculate that the presence of the Asn in TM1 may provide Cl^--coupled SLC6 transporters not only with the opportunity to more efficiently tap the Na^+ gradient for uphill transport but also allows transporters to move between coupled transporter modes of substrate conduction and channel-like modes of neurotransmitter transport.

Acknowledgments—We thank Nathan Burbach and Kris Pavlish for technical assistance.

REFERENCES

1. Kanner, B. I., and Schuldiner, S. (1987) *CRC Crit. Rev. Biochem.* **22,** 1–38
2. Ramamoorthy, S., Bauman, A. L., Moore, K. R., Han, H., Yang-Feng, T., Chang, A. S., Ganapathy, V., and Blakely, R. D. (1993) *Proc. Natl. Acad. Sci. U.S.A.* **90,** 2542–2546
3. Danbolt, N. C., Storm-Mathisen, J., and Kanner, B. I. (1992) *Neuroscience* **51,** 295–310
4. Kanai, Y., Stelzner, M. G., Lee, W. S., Wells, R. G., Brown, D., and Hediger, M. A. (1992) *Am. J. Physiol.* **263,** F1087–F1092
5. Barker, E. L., and Blakely, R. D. (1995) in *Psychopharmacology: The Fourth Generation of Progress* (Bloom, F. E., and Kupfer, D. J., eds) pp. 321–333, Raven Press, Ltd., New York
6. Mitchell, P. (1961) *Nature* **191,** 144–148
7. Rudnick, G. (2002) in *Transmembrane Transporters* (Quick, M. W., ed) pp. 125–141, Wiley-Liss, Inc., New York
8. Nelson, M. T., and Blaustein, M. P. (1982) *J. Membr. Biol.* **69,** 213–223
9. Lingjaerde, O., Jr. (1971) *Acta Physiol. Scand.* **81,** 75–83
10. Quick, M. W. (2003) *Neuron* **40,** 537–549
11. Adams, S. V., and DeFelice, L. J. (2002) *Biophys. J.* **83,** 3268–3282
12. Ramsey, I. S., and DeFelice, L. J. (2002) *J. Biol. Chem.* **277,** 14475–14482
13. Lin, F., Lester, H. A., and Mager, S. (1996) *Biophys. J.* **71,** 3126–3135
14. Carvelli, L., McDonald, P. W., Blakely, R. D., and Defelice, L. J. (2004) *Proc. Natl. Acad. Sci. U.S.A.* **101,** 16046–16051
15. Ingram, S. L., Prasad, B. M., and Amara, S. G. (2002) *Nat. Neurosci.* **5,** 971–978
16. Binda, F., Dipace, C., Bowton, E., Robertson, S. D., Lute, B. J., Fog, J. U., Zhang, M., Sen, N., Colbran, R. J., Gnegy, M. E., Gether, U., Javitch, J. A., Erreger, K., and Galli, A. (2008) *Mol. Pharmacol.* **74,** 1101–1108
17. Carvelli, L., Blakely, R. D., and DeFelice, L. J. (2008) *Proc. Natl. Acad. Sci. U.S.A.* **105,** 14192–14197
18. Hoffman, B. J., and Mezey, E. (1989) *FEBS Lett.* **247,** 453–462
19. Schroeter, S., and Blakely, R. D. (1996) *Ann. N.Y. Acad. Sci.* **801,** 239–255
20. Adragna, N. C., Di Fulvio, M., and Lauf, P. K. (2004) *J. Membr. Biol.* **201,** 109–137
21. Jang, I. S., Jeong, H. J., and Akaike, N. (2001) *J. Neurosci.* **21,** 5962–5972
22. Yamashita, A., Singh, S. K., Kawate, T., Jin, Y., and Gouaux, E. (2005) *Nature* **437,** 215–223
23. Shaffer, P. L., Goehring, A., Shankaranarayanan, A., and Gouaux, E. (2009) *Science* **325,** 1010–1014
24. Ressl, S., Terwisscha van Scheltinga, A. C., Vonrhein, C., Ott, V., and Ziegler, C. (2009) *Nature* **458,** 47–52
25. Faham, S., Watanabe, A., Besserer, G. M., Cascio, D., Specht, A., Hirayama, B. A., Wright, E. M., and Abramson, J. (2008) *Science* **321,** 810–814
26. Weyand, S., Shimamura, T., Yajima, S., Suzuki, S., Mirza, O., Krusong, K., Carpenter, E. P., Rutherford, N. G., Hadden, J. M., O'Reilly, J., Ma, P., Saidijam, M., Patching, S. G., Hope, R. J., Norbertczak, H. T., Roach, P. C., Iwata, S., Henderson, P. J., and Cameron, A. D. (2008) *Science* **322,** 709–713
27. Abramson, J., and Wright, E. M. (2009) *Curr. Opin. Struct. Biol.* **19,** 425–432
28. Henry, L. K., Adkins, E. M., Han, Q., and Blakely, R. D. (2003) *J. Biol. Chem.* **278,** 37052–37063
29. Blakely, R. D., Berson, H. E., Fremeau, R. T., Jr., Caron, M. G., Peek, M. M., Prince, H. K., and Bradley, C. C. (1991) *Nature* **354,** 66–70
30. Adams, S. V., and DeFelice, L. J. (2003) *Biophys. J.* **85,** 1548–1559
31. Petersen, C. I., and DeFelice, L. J. (1999) *Nat. Neurosci.* **2,** 605–610
32. Kaufmann, K. W., Dawson, E. S., Henry, L. K., Field, J. R., Blakely, R. D., and Meiler, J. (2009) *Proteins* **74,** 630–642
33. Zomot, E., Bendahan, A., Quick, M., Zhao, Y., Javitch, J. A., and Kanner, B. I. (2007) *Nature* **449,** 726–730
34. Forrest, L. R., Tavoulari, S., Zhang, Y. W., Rudnick, G., and Honig, B. (2007) *Proc. Natl. Acad. Sci. U.S.A.* **104,** 12761–12766
35. Bayly, C. I., and Kollman, P. A. (1994) *J. Am. Chem. Soc.* **116,** 697–703
36. Anisimov, V. M., Lamoureux, G., Vorobyov, I. V., Huang, N., Roux, B., and MacKerell Jr., A. D. (2005) *J. Chem. Theory Comput.* **1,** 153–168
37. Foloppe, N., and Nilsson, L. (2007) *J. Mol. Biol.* **372,** 798–816
38. Canutescu, A. A., Shelenkov, A. A., and Dunbrack, R. L., Jr. (2003) *Protein Sci.* **12,** 2001–2014
39. Jo, S., Lim, J. B., Klauda, J. B., and Im, W. (2009) *Biophys. J.* **97,** 50–58
40. Phillips, J. C., Braun, R., Wang, W., Gumbart, J., Tajkhorshid, E., Villa, E., Chipot, C., Skeel, R. D., Kalé, L., and Schulten, K. (2005) *J. Comput. Chem.* **26,** 1781–1802
41. Brooks, B. R., Brooks, C. L., 3rd, Mackerell, A. D., Jr., Nilsson, L., Petrella,

R. J., Roux, B., Won, Y., Archontis, G., Bartels, C., Boresch, S., Caflisch, A., Caves, L., Cui, Q., Dinner, A. R., Feig, M., Fischer, S., Gao, J., Hodoscek, M., Im, W., Kuczera, K., Lazaridis, T., Ma, J., Ovchinnikov, V., Paci, E., Pastor, R. W., Post, C. B., Pu, J. Z., Schaefer, M., Tidor, B., Venable, R. M., Woodcock, H. L., Wu, X., Yang, W., York, D. M., and Karplus, M. (2009) *J. Comput. Chem.* **30,** 1545–1614
42. Caplan, D. A., Subbotina, J. O., and Noskov, S. Y. (2008) *Biophys. J.* **95,** 4613–4621
43. Noskov, S. Y. (2008) *Proteins* **73,** 851–863
44. Chang, A. S., and Lam, D. M. (1998) *J. Physiol.* **510,** 903–913
45. Barker, E. L., Moore, K. R., Rakhshan, F., and Blakely, R. D. (1999) *J. Neurosci.* **19,** 4705–4717
46. Chen, J. G., Liu-Chen, S., and Rudnick, G. (1997) *Biochemistry* **36,** 1479–1486
47. Chen, J. G., Sachpatzidis, A., and Rudnick, G. (1997) *J. Biol. Chem.* **272,** 28321–28327
48. Ni, Y., McPhie, P., Deacon, A., Ealick, S., and Coleman, W. G., Jr. (2001) *J. Biol. Chem.* **276,** 27329–27334
49. Mitchell, S. M., Lee, E., Garcia, M. L., and Stephan, M. M. (2004) *J. Biol. Chem.* **279,** 24089–24099
50. Forrest, L. R., Zhang, Y. W., Jacobs, M. T., Gesmonde, J., Xie, L., Honig, B. H., and Rudnick, G. (2008) *Proc. Natl. Acad. Sci. U.S.A.* **105,** 10338–10343
51. Zhang, Y. W., and Rudnick, G. (2006) *J. Biol. Chem.* **281,** 36213–36220
52. Cao, Y., Li, M., Mager, S., and Lester, H. A. (1998) *J. Neurosci.* **18,** 7739–7749
53. Hilber, B., Scholze, P., Dorostkar, M. M., Sandtner, W., Holy, M., Boehm, S., Singer, E. A., and Sitte, H. H. (2005) *Neuropharmacology* **49,** 811–819
54. Corey, J. L., Quick, M. W., Davidson, N., Lester, H. A., and Guastella, J. (1994) *Proc. Natl. Acad. Sci. U.S.A.* **91,** 1188–1192
55. Mager, S., Cao, Y., and Lester, H. A. (1998) *Methods Enzymol.* **296,** 551–566
56. Mager, S., Min, C., Henry, D. J., Chavkin, C., Hoffman, B. J., Davidson, N., and Lester, H. A. (1994) *Neuron* **12,** 845–859
57. Sonders, M. S., Zhu, S. J., Zahniser, N. R., Kavanaugh, M. P., and Amara, S. G. (1997) *J. Neurosci.* **17,** 960–974
58. Nelson, P. J., and Rudnick, G. (1982) *J. Biol. Chem.* **257,** 6151–6155
59. Ben-Yona, A., Bendahan, A., and Kanner, B. I. (2011) *J. Biol. Chem.* **286,** 2826–2833
60. Tavoulari, S., Rizwan, A. N., Forrest, L. R., and Rudnick, G. (2011) *J. Biol. Chem.* **286,** 2834–2842
61. Meiler, J., and Baker, D. (2006) *Proteins* **65,** 538–548
62. Adkins, E. M., Barker, E. L., and Blakely, R. D. (2001) *Mol. Pharmacol.* **59,** 514–523
63. Barker, E. L., Perlman, M. A., Adkins, E. M., Houlihan, W. J., Pristupa, Z. B., Niznik, H. B., and Blakely, R. D. (1998) *J. Biol. Chem.* **273,** 19459–19468
64. Field, J. R., Henry, L. K., and Blakely, R. D. (2010) *J. Biol. Chem.* **285,** 11270–11280
65. Swanson, J. M., Henchman, R. H., and McCammon, J. A. (2004) *Biophys. J.* **86,** 67–74
66. Simonson, T., Carlsson, J., and Case, D. A. (2004) *J. Am. Chem. Soc.* **126,** 4167–4180
67. Li, L., Vorobyov, I., and Allen, T. W. (2008) *J. Phys. Chem. B* **112,** 9574–9587
68. Beuming, T., Kniazeff, J., Bergmann, M. L., Shi, L., Gracia, L., Raniszewska, K., Newman, A. H., Javitch, J. A., Weinstein, H., Gether, U., and Loland, C. J. (2008) *Nat. Neurosci.* **11,** 780–789
69. Screpanti, E., and Hunte, C. (2007) *J. Struct. Biol.* **159,** 261–267
70. Celik, L., Sinning, S., Severinsen, K., Hansen, C. G., Møller, M. S., Bols, M., Wiborg, O., and Schiøtt, B. (2008) *J. Am. Chem. Soc.* **130,** 3853–3865
71. Shimamura, T., Weyand, S., Beckstein, O., Rutherford, N. G., Hadden, J. M., Sharples, D., Sansom, M. S., Iwata, S., Henderson, P. J., and Cameron, A. D. (2010) *Science* **328,** 470–473
72. Watanabe, A., Choe, S., Chaptal, V., Rosenberg, J. M., Wright, E. M., Grabe, M., and Abramson, J. (2010) *Nature* **468,** 988–991
73. Beuming, T., Shi, L., Javitch, J. A., and Weinstein, H. (2006) *Mol. Pharmacol.* **70,** 1630–1642
74. Fog, J. U., Khoshbouei, H., Holy, M., Owens, W. A., Vaegter, C. B., Sen, N., Nikandrova, Y., Bowton, E., McMahon, D. G., Colbran, R. J., Daws, L. C., Sitte, H. H., Javitch, J. A., Galli, A., and Gether, U. (2006) *Neuron* **51,** 417–429
75. Galli, A., Blakely, R. D., and DeFelice, L. J. (1998) *Proc. Natl. Acad. Sci. U.S.A.* **95,** 13260–13265
76. Sung, U., and Blakely, R. D. (2007) *Mol. Cell. Neurosci.* **34,** 251–260